



Thermo-mechanical stability of multi-scale-architected thin-film-based solid oxide fuel cells assessed by thermal cycling tests

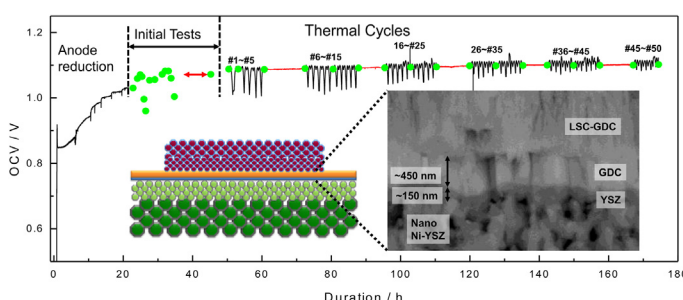
Ho-Sung Noh, Kyung Joong Yoon, Byung-Kook Kim, Hae-June Je, Hae-Weon Lee, Jong-Ho Lee, Ji-Won Son*

High-temperature Energy Materials Research Center, Korea Institute of Science and Technology, Hwarangno 14-gil 5, Seongbuk-gu, Seoul 136-791, Republic of Korea

HIGHLIGHTS

- Improved thermo-mechanical stability of thin film-SOFCs (TF-SOFCs) is reported.
- The TF-SOFC is composed of a 600-nm-thick electrolyte and nano-structured electrodes.
- Multi-scale-architecture enables the TF-SOFC to survive 50 thermal cycles (TCs).
- The TF-SOFC sustains a peak power density over 1 W cm^{-2} at 600°C after 50 TCs.
- The whole cell comes out intact after over 150 h of operation and 50 TCs.

GRAPHICAL ABSTRACT



ARTICLE INFO

Article history:

Received 8 August 2013
Received in revised form
21 October 2013
Accepted 23 October 2013
Available online 1 November 2013

Keywords:

Solid oxide fuel cell
Thin-film electrolyte
Nanostructured electrode
Multi-scale architecture
Thermal cycle

ABSTRACT

The thermo-mechanical stability of a thin-film and nanostructure-based SOFC (TF-SOFC) is assessed by thermal cycling tests. An ultrathin bi-layer electrolyte composed of 150-nm-thick yttria-stabilized zirconia (YSZ) and 450-nm-thick gadolinia-doped ceria (GDC) is successfully built on a NiO-YSZ anode support the microstructure scale of which changes from μm to nm (multi-scale architecture). The concept of multi-scale architecture in the TF-SOFC not only enables the reliable implementation of thin-film electrolytes and nanostructured electrodes to improve the critical low-temperature performance of the SOFC but also secures the thermo-mechanical stability of TF-SOFC. Competent cell performance is obtained, including a peak power density about 1.4 W cm^{-2} at 600°C . The TF-SOFC survives 50 thermal cycle tests between 600 and 400°C over 124 h without suffering a drastic failure. Although some cell output degradation is observed after the thermal cycling tests, the cell sustains a peak power density over 1 W cm^{-2} at 600°C , which indicates the superior thermo-mechanical stability of the multi-scale-architected TF-SOFC.

© 2013 Elsevier B.V. All rights reserved.

1. Introduction

In the field of solid oxide fuel cell (SOFC) research, thin-film and nanostructured components are being implemented at an ever-

increasing rate. In conventional, powder-processed SOFCs, thin-film components are often employed to avoid high processing temperatures that would cause chemical reactions between the cell components, e.g., a ceria-base barrier layer [1–3]. More serious applications of thin-film components, however, have been attempts to develop micro-SOFCs based on micro electro-mechanical system (MEMS) techniques [4–11] and to improve the performance

* Corresponding author. Tel.: +82 2 958 5530; fax: +82 2 958 5529.
E-mail addresses: jiwon.son@gmail.com, jwson@kist.re.kr (J.-W. Son).

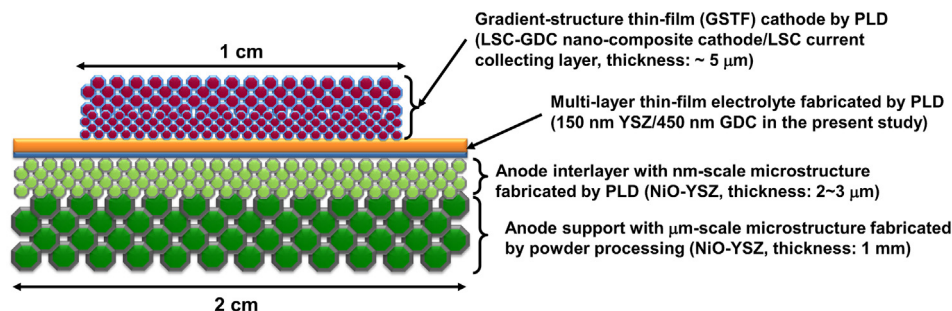


Fig. 1. A schematic showing the concept of the multi-scale-architected TF-SOFC. The dimensions of the TF-SOFC in the present report are listed.

of low-temperature-operation SOFCs (LT-SOFCs) [12–18]. In particular, MEMS-based micro-SOFCs have attracted attention due to their remarkably high performance at low temperatures including peak power densities over 1 W cm^{-2} at 500°C [4,8].

Nevertheless, the extremely poor thermo-mechanical stability of the free-standing MEMS platform and the unbearably short lifetime caused by the instability of the nano-porous noble metal electrodes have made this technology unrealistic so far. Very few results have been reported regarding the lifetime or degradation of cells based on this technology [7], and the level of degradation (more than 50% in 12 h at 400°C [8]) of micro-SOFCs in those reports is far from that needed for practical application. In a previous study by the authors [10], it was shown that a supporting porous structure made out of anodized aluminum oxide (AAO) could improve the degradation level to less than 10% after 17 h (1000 min). Although this was quite a substantial improvement, the degradation is still quite serious.

To alleviate the thermo-mechanical frailty while at the same time obtaining the significantly enhanced low-temperature performance of thin-film and nanostructure-based SOFCs (denoted as TF-SOFCs), the authors investigated the TF-SOFCs built on conventional anode supports in previous reports [12–14]. Through optimization and improvements, peak power densities exceeding 500 mW cm^{-2} at 500°C in an active area of 1 cm by 1 cm can now routinely be obtained [19]. These achievements were possible by realizing the cell platform based on ‘multi-scale architecture’.

In Fig. 1, a schematic shows the concept of multi-scale architecture. The main structural support is fabricated using conventional powder processing and consists of micrometer-scale grains. The anode interlayer, which consists of nanometer-scale grains, is fabricated using thin-film processing (pulsed laser deposition, PLD, in this case) over the anode support to complete the combination of micro to nano-scale (multi-scale) microstructures at the anode. A bi-layer thin-film electrolyte having a thickness less than $1 \mu\text{m}$ is formed over the nanostructure interlayer. The cathode is composed of a multi-layer structure as well. Nano-composite layers composed of the mixture of electrolyte and electrode materials are deposited using PLD. By controlling the ambient pressure during deposition, a porosity-gradient structure can be realized in the nano-composite cathode [20]. The top layer is a single electrode material layer that functions as a current collecting layer. The lateral dimensions of the cell are at the cm level, so the whole cell contains multiple scales of physical dimensions (cm–mm– μm –nm). This concept is denoted as multi-scale architecture.

There are several critical features that are expected to remarkably improve the thermo-mechanical stability of TF-SOFCs based on multi-scale architecture. First, the ultrathin electrolyte exhibits greatly improved stability in comparison with the free-standing membrane because it is supported by the nano-porous structure. Second, the porosity-gradient structure at both the anode and cathode will sandwich the ultrathin electrolyte; as a result, stronger

electrolyte/electrode interfaces can be produced. In addition, the anode and cathode are composed of nano-composites of the electrode and electrolyte materials. Because this composite material is not simply a single material or a nano-porous noble metal, the degradation of the cell is expected to be suppressed to quite an extent.

Even in light of all of these facts, an investigation regarding the durability of a multi-scale-architected TF-SOFC has never before been quantitatively performed. Therefore, in the present article, the thermo-mechanical stability of the cells on this platform is reported. To assess the thermo-mechanical stability of the multi-

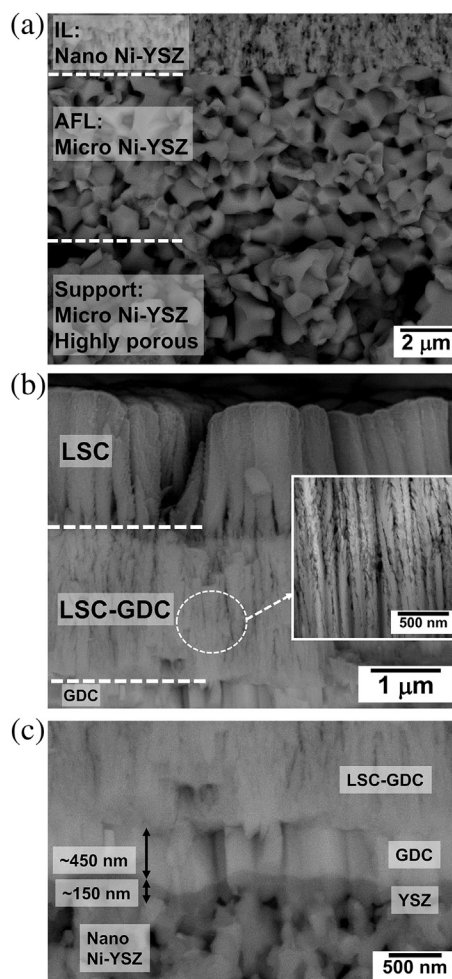


Fig. 2. Cross-sectional SEM micrographs showing (a) the anode structure; (b) the cathode structure (inset shows the porosity-gradient structure at the junction of LSC-GDC layers); and (c) the bi-layer electrolyte structure of the multi-scale-architected TF-SOFC presented in this study (taken after the cell test).

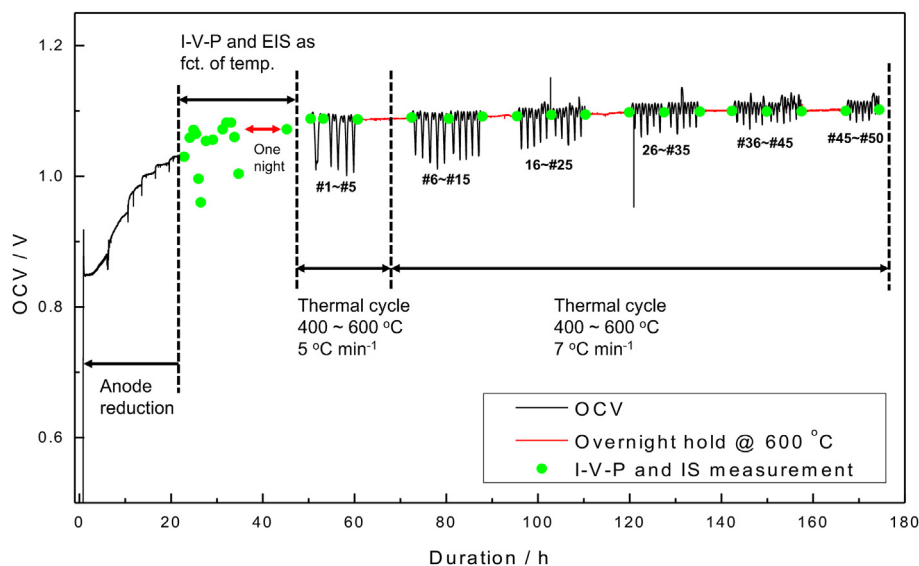


Fig. 3. The OCV change over the course of thermal cell testing.

scale-architected TF-SOFC, thermal cycling tests were performed after the initial cell performance tests, and the change in cell performance as a function of number of thermal cycles was monitored.

2. Experimental

TF-SOFCs based on a 150-nm-thick YSZ reduction blocking layer and a 450-nm-thick GDC electrolyte layer (bi-layer electrolyte) were fabricated on a compression-molded NiO-YSZ anode support with a screen-printed anode functional layer (C-SP anode). These C-SP anode supports were sintered at 1400 °C for 3 h. An approximately 3- μ m-thick NiO-YSZ nano-composite interlayer was deposited over the C-SP support using PLD at a substrate temperature (T_s) of 700 °C and an ambient pressure (P_{amb}) for oxygen of 6.67 Pa. Afterward, the whole support structure was annealed at 1200 °C for 1 h to prevent Ni agglomeration during the reduction at the interlayer [21]. Both YSZ and GDC thin films were deposited over the interlayer at $T_s = 700$ °C and $P_{amb} = 6.67$ Pa. The process conditions for the TF-SOFC on the C-SP support are consistent with those from a previous work [13].

The cathode is composed of three layers and uses lanthanum strontium cobaltite (LSC) as the electrode material: (1) a $\text{La}_{0.6}\text{Sr}_{0.4}\text{CoO}_{3-\delta}$ (LSC64)-GDC nano-composite layer deposited at $T_s = 700$ °C and $P_{amb} = 26.7$ Pa; (2) an LSC64-GDC nano-composite layer deposited at $T_s = 700$ °C and $P_{amb} = 40$ Pa; and (3) an LSC64 single layer deposited at room temperature and $P_{amb} = 13.3$ Pa. The LSC64-GDC nano-composite layers were deposited using an LSC64-GDC composite target prepared by sintering a compacted mixed LSC64 and GDC powder pellet (mixing volume ratio = 1:1) at 1200 °C for 5 h. After deposition of the multilayer cathode, the entire cell was post-annealed at 650 °C for 1 h to crystallize the top LSC64 layer. The resulting cathode thickness was approximately 4.5 μ m. The fabrication process for the gradient-structure thin-film (GSTF) cathode was also described in a previous work [20]. The microstructure of each cell was observed via scanning electron microscopy (SEM, XL-30 and Inspect F50, FEI).

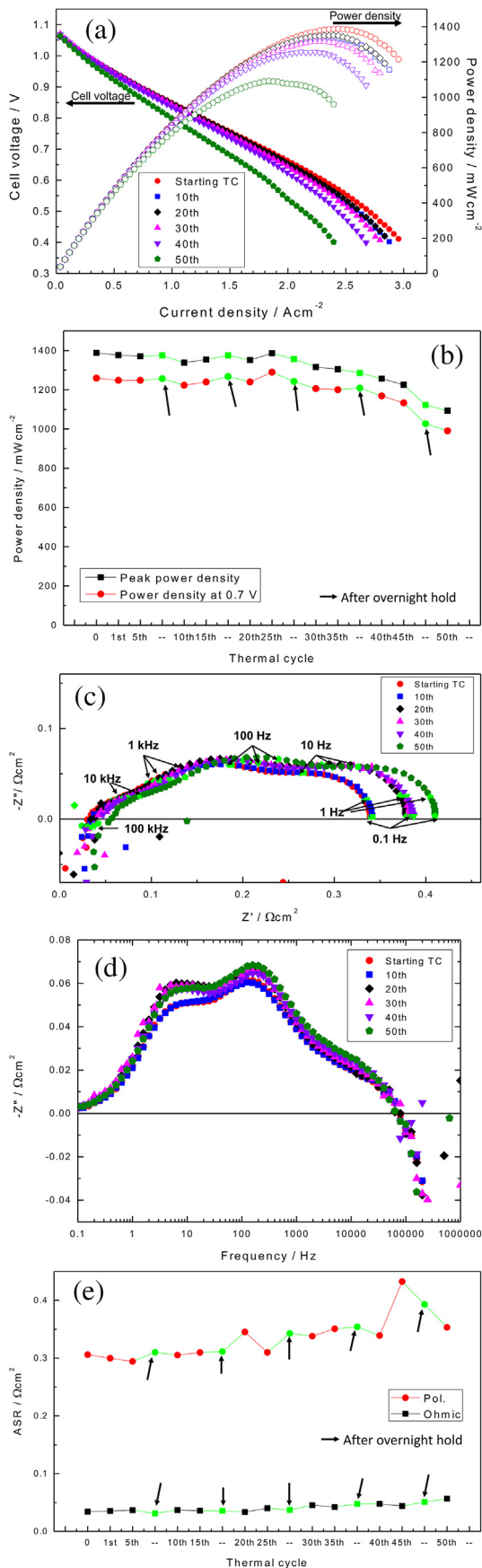
To operate the fuel cell, air and humidified H_2 (3% H_2O) were used as the oxidant and fuel, respectively, and the flow rates of each were held constant at 200 sccm. A modified rib design of the interconnect was used for the cell test with gold meshes having openings of 250 μ m by 250 μ m. The cell test configuration with reduced contact loss was described in detail in a previous work

[22]. The cell's operating temperature varied from 650 to 400 °C at intervals of 50 °C, and electrochemical impedance spectra (EIS) and current-voltage-power (I - V - P) curves were obtained at each temperature. A Solartron impedance analyzer with an electrochemical interface (SI1260 and SI1287, Solartron) and an Iviumstat electrochemical analyzer (Iviumstat, Ivium Technologies) were used to obtain these EIS and I - V - P curves, and each EIS was observed over a frequency range from 10^6 Hz to 10^{-1} Hz. The AC amplitude of the impedance measurements was 50 mV.

After observing cell performance as a function of temperature, thermal cycle tests between 600 and 400 °C were performed. The temperature was not cooled below 400 °C because the furnace temperature of the cell test setup could not follow the cooling rate. For the first 5 cycles, the heating and cooling rate was 5 °C min^{-1} . The first 5 cycles were performed over one day and the heating and cooling rate was changed to 7 °C min^{-1} for the next day onward. The change of the cooling rate and the number of the thermal cycles per day is to accelerate the thermal cycling condition after the feasibility test on initial and milder test conditions on day 1. A total of 50 thermal cycle tests were completed before the end of the measurement. After every 5 thermal cycles and after every overnight, EIS and I - V - P measurements were acquired at 600 °C.

3. Results and discussion

In Fig. 2, cross-sectional SEM micrographs of the components of the multi-scale-architected TF-SOFC after the cell test are shown. In Fig. 2(a), the multi-scale anode substrate composed of the Ni-YSZ support with micron-level grain sizes (micro Ni-YSZ) and the Ni-YSZ interlayer with nanometer-level grain sizes (nano Ni-YSZ) is clearly displayed. Because the anode has been reduced, NiO-YSZ changed into Ni-YSZ. As described in the experimental section, the C-SP anode support is composed of a compression-molded and highly porous anode substrate and a screen-printed anode functional layer (AFL). The nanostructured Ni-YSZ interlayer fabricated by PLD is the top layer of the anode and supports the ultrathin electrolyte. In Fig. 2(b), the layered structure of the GSTF cathode is shown. Because the interface between neighboring LSC-GDC layers having different porosities is rather unclear, a micrograph of high-angle annular dark field (HAADF) transmission electron microscopy (TEM) is shown in an inset figure. This figure clearly shows that a lower-to-higher porosity gradient structure is formed in the



cathode from the interface of the cathode and the electrolyte to the top surface. The porosity-gradient structures realized both at the anode and the cathode are expected to augment the thermo-mechanical stability of the electrolyte.

In Fig. 2(c), the bi-layer electrolyte is shown. Although the electrolyte exhibits a columnar grain structure, through-pinholes or through-cracks are not formed and a dense, gas-impermeable ultrathin bi-layer electrolyte layer is fabricated. The ultrathin bi-layer electrolyte does not exhibit any serious fracture or rupture after the long duration of the test, which indicates that the multi-scale architecture sustained the integrity of the TF-SOFC successfully. Moreover, the composite approach to fabricating the anode and cathode enhanced the material similarity between the electrolyte and the electrodes (the bottom YSZ electrolyte layer to YSZ in the Ni-YSZ interlayer and the top GDC electrolyte layer to GDC in the LSC-GDC layer), which is also expected to support the structural stability of the ultrathin electrolyte.

In Fig. 3, the open circuit voltage (OCV) change as a function of the monitoring duration is marked from the start of the anode reduction process. The cell OCV values are close to 1.1 V at 600 °C. This value is slightly lower than the theoretical OCV value at the condition (~ 1.13 V), may indicate the existence of the pinholes at the thin electrolyte, but it is a high value considering the thinness of the electrolyte. This result indicates that the 150-nm-thick YSZ blocking layer was formed without major defects and successfully blocked the reduction of the GDC layer over the entire active area (1 cm by 1 cm) as in a former study by the authors [12]. Two separate cell performance tests were executed while changing the temperature between 650 and 400 °C. Very high cell performance was observed in the present study for the anode-supported SOFC using a thin-film electrolyte and nanostructured electrodes; notably, peak power densities of $\approx 1.4 \text{ W cm}^{-2}$ at 600 °C and $\approx 0.5 \text{ W cm}^{-2}$ at 500 °C were observed. The samples were held at 600 °C for one night (approximately 12 h) following the initial cell tests, and even though these processes lasted approximately 24 h, no discernible cell performance degradation was observed.

After the initial screening of the cell performance, the thermo-mechanical stability of the cell was put to the test by practicing thermal cycling. Fifty thermal cycling tests lasted for 6 days. In terms of the OCV, there was no deterioration or degradation as can be seen in Fig. 3, which indicates the high physical integrity of the cell and especially of the ultrathin (600 nm) bi-layer electrolyte membrane. Considering that the MEMS-based free-standing electrolyte membrane can easily fail due to processing conditions or slight temperature changes [9,23], the thermo-mechanical stability of the multi-scale-architected TF-SOFC can be said to have reached a significant level for thin-film and nanostructure-based SOFCs.

Fig. 4 shows the performance change during the tests. Fig. 4(a) shows the I - V - P curves after every 10 cycles while Fig. 4(b) shows changes to the power densities during the thermal cycling tests. Fig. 4(c) and (d) displays Nyquist plots and Bode plots of the EIS after every 10 cycles, respectively. Fig. 4(e) displays changes in the ASR values from the Nyquist plots. After 50 thermal cycles, the cell still exhibited a peak power density over 1 W cm^{-2} at 600 °C, which is a substantially high power output for anode-supported SOFCs (Fig. 4(a)). The peak power density changed from 1388 to 1092 W cm^{-2} , and the power density at 0.7 V changed from 1259 to 990 W cm^{-2} over the course of the thermal cycling tests (Fig. 4(b)). Because it took 124 h to complete the 50 thermal cycles, the

Fig. 4. Cell performance change during the thermal cycling test: (a) I - V - P curves after every 10 thermal cycles; (b) power density changes; (c) Nyquist plots of EIS changes after every 10 thermal cycles; (d) Bode plots of EIS changes after every 10 thermal cycles; and (e) ASR changes.

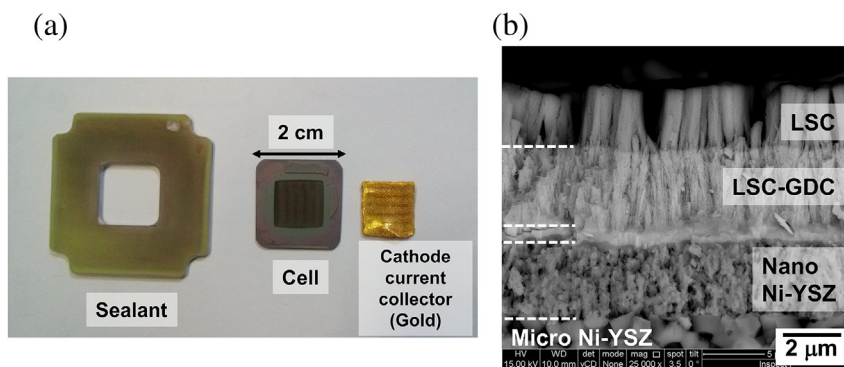


Fig. 5. (a) Digital photographs of the cell test components after the cell test and (b) the overall cross-sectional microstructure of the tested cell.

degradation rate is approximately 17%/100 h. Considering the degradation rates of common micro-SOFCs employing thin-film and nanostructured components ($>50\%/12$ h at 400°C [8]), this milestone represents substantial progress. In addition, the cell was put through the thermal cycling test and was kept at 600°C during the holding time; these conditions are extremely harsh for thin film and nanostructured components. It is certain that the concept of multi-scale architecture is a valid approach to significantly improve the thermo-mechanical stability of the TF-SOFC.

The EIS changes shown in Fig. 4(c)–(e) indicate that, despite several outliers (e.g., the 20th and 45th cycles), a gradual degradation occurred while the thermal cycling tests progressed. In Fig. 4(c), it is noted that the shapes of the Nyquist plot do not change much as the thermal cycling tests progress. This indicates that there is no drastic change in the electrode reaction mechanism although the degradation progresses. Bode plots shown in Fig. 4(d) demonstrate that the degradation of the polarization ASR in the frequency range from 1 to 10 Hz occurs faster than that of other frequency ranges. This frequency range is generally known to be affected by the gas transport [19,24], but recent findings indicate that especially for the thin-film processed cathode [25–29], this range is closely related to the surface reaction of the cathode. Therefore, it is postulated that cathode degradation, such as the coalescence of the particles of the cathode nano-composite or the chemical degradation of the cathode surface, could be the major factor that contributes to performance degradation. Fig. 4(e) implies that the degradation of the polarization ASR is more significant than that of the ohmic ASR. The slight increment in terms of the ohmic ASR can be caused by several reasons, such as the change of the contact loss, the interface adhesion, and/or chemical degradation, but it does not affect the overall cell performance degradation as significant as the electrode polarization ASR. In a previous work by the authors [19], it was asserted that the most important improvement to achieve ultimate performance in TF-SOFCs is to develop electrodes with high performance to reduce the polarization ASR. The current result shows that a high-quality electrode is important not only in terms of performance but also for stability. To attain suppressed degradation of the TF-SOFC, it is believed that an electrode with high thermo-mechanical stability is required.

Digital photographs of the cell test components after the cell test are shown in Fig. 5(a), and the overall cross-sectional microstructure of the cell is shown in Fig. 5(b). Every component survived the harsh tests without drastic failure and came out intact. In fact, this result proves the survival capability of both the TF-SOFC and the sealant [30] during thermal cycling; these are two key components of the actual SOFC stack. Therefore, it can be asserted that the current study lays the groundwork to eventually employ thin-film and nanostructured components to practical working SOFC devices.

4. Conclusions

The concept of multi-scale architecture in TF-SOFCs not only improves critical performance of the anode-supported SOFC but also secures the thermo-mechanical stability of the TF-SOFC. Competent cell performance, such as peak power densities about 1.4 W cm^{-2} at 600°C , was obtained in a TF-SOFC based on an ultrathin 150-nm-thick YSZ/450-thick-nm GDC bi-layer electrolyte built on a μm -to-nm multi-scale-architected anode support. The TF-SOFC survived 50 thermal cycling tests over the course of 124 h without suffering a drastic failure. The thermo-mechanical stability of the multi-scale-architected TF-SOFCs is significantly greater when compared to other TF-SOFCs, such as MEMS-based micro-SOFCs. Although this approach cannot be said to be mature at the current stage, the present study suggests a highly potent pathway towards practical employment of thin-film and nanostructured components in SOFC technology.

Acknowledgments

This work was financially supported by the Young Fellow Program of KIST, the Global Frontier R&D Program on Center for Multiscale Energy Systems (2011-0031579) and the Mid-career Researcher Program (2011-0012230) funded by the National Research Foundation under the Ministry of Science, ICT & Future, Korea.

References

- [1] R. Steinberger-Wilckens, L. Blum, H.-P. Buchkremer, B.d. Haart, J. Malzbender, M. Pap, ECS Trans. 35 (2011) 53–60.
- [2] N. Christiansen, H. Holm-Larsen, S. Primdahl, M. Wandel, S. Ramousse, A. Hagen, ECS Trans. 35 (2011) 71–80.
- [3] T. Franco, M. Haydn, R. Mücke, A. Weber, M. Rüttiger, O. Büchler, S. Uhlenbruck, N.H. Menzler, A. Venskutonis, L.S. Sigl, ECS Trans. 35 (2011) 343–349.
- [4] C.-C. Chao, C.-M. Hsu, Y. Cui, F.B. Prinz, ACS Nano 5 (2011) 5692–5696.
- [5] H. Huang, M. Nakamura, P.C. Su, R. Fasching, Y. Saito, F.B. Prinz, J. Electrochem. Soc. 154 (2007) B20–B24.
- [6] D. Beckel, A. Bieberle-Hutter, A. Harvey, A. Infortuna, U.P. Muecke, M. Prestat, J.L.M. Rupp, L.J. Gauckler, J. Power Sources 173 (2007) 325–345.
- [7] A. Evans, A. Bieberle-Hütter, J.L.M. Rupp, L.J. Gauckler, J. Power Sources 194 (2009) 119–129.
- [8] K. Kerman, B.-K. Lai, S. Ramanathan, J. Power Sources 196 (2011) 2608–2614.
- [9] M. Tsuchiya, B.-K. Lai, S. Ramanathan, Nat. Nanotechnol. 6 (2011) 282–286.
- [10] C.-W. Kwon, J.-I. Lee, K.-B. Kim, H.-W. Lee, J.-H. Lee, J.-W. Son, J. Power Sources 210 (2012) 178–183.
- [11] C.-W. Kwon, J.-W. Son, J.-H. Lee, H.-M. Kim, H.-W. Lee, K.-B. Kim, Adv. Funct. Mater. 21 (2011) 1154–1159.
- [12] D.-H. Myung, J. Hong, K. Yoon, B.-K. Kim, H.-W. Lee, J.-H. Lee, J.-W. Son, J. Power Sources 206 (2012) 91–96.
- [13] H.-S. Noh, H. Lee, B.-K. Kim, H.-W. Lee, J.-H. Lee, J.-W. Son, J. Power Sources 196 (2011) 7169–7174.
- [14] H.-S. Noh, J.-W. Son, H. Lee, H.-S. Song, H.-W. Lee, J.-H. Lee, J. Electrochem. Soc. 156 (2009) B1484–B1490.
- [15] J.H. Joo, G.M. Cho, Solid State Ionics 178 (2007) 1602–1607.
- [16] J.H. Joo, G.M. Choi, J. Power Sources 182 (2008) 589–593.

- [17] T. Suzuki, M.H. Zahir, T. Yamaguchi, Y. Fujishiro, M. Awano, N. Sammes, *J. Power Sources* 195 (2010) 7825–7828.
- [18] T. Ishihara, H. Eto, J. Yan, *Int. J. Hydrogen Energy* 36 (2011) 1862–1867.
- [19] H.-S. Noh, K.J. Yoon, B.-K. Kim, H.-J. Je, H.-W. Lee, J.-H. Lee, J.-W. Son, *J. Power Sources* 247 (2014) 105–111.
- [20] D.-H. Myung, J. Hwang, J. Hong, H.-W. Lee, B.-K. Kim, J.-H. Lee, J.-W. Son, *J. Electrochem. Soc.* 158 (2011) B1000–B1006.
- [21] H.-S. Noh, J.-W. Son, H. Lee, H.-I. Ji, J.-H. Lee, H.-W. Lee, *J. Eur. Ceram. Soc.* 30 (2010) 3415–3423.
- [22] H.-S. Noh, J. Hwang, K. Yoon, B.-K. Kim, H.-W. Lee, J.-H. Lee, J.-W. Son, *J. Power Sources* 230 (2013) 109–114.
- [23] A. Evans, M. Prestat, R. Tölke, M.V.F. Schlupp, L.J. Gauckler, Y. Safa, T. Hocker, J. Courbat, D. Briand, N.F. de Rooij, D. Courty, *Fuel Cells* 12 (2012) 614–623.
- [24] J. Hwang, H. Lee, K.J. Yoon, H.-W. Lee, B.-K. Kim, J.-H. Lee, J.-W. Son, *J. Electrochem. Soc.* 159 (2012) F639–F643.
- [25] J.-H. Park, W.-S. Hong, G.C. Kim, H.J. Chang, J.-H. Lee, K.J. Yoon, J.-W. Son, *J. Electrochem. Soc.* 160 (2013) F1027–F1032.
- [26] P. Plonczak, M. Søgaard, A. Bieberle-Hütter, P.V. Hendriksen, L.J. Gauckler, *J. Electrochem. Soc.* 159 (2012) B471–B482.
- [27] F.S. Baumann, J. Fleig, H.-U. Habermeier, J. Maier, *Solid State Ionics* 177 (2006) 1071–1081.
- [28] T. Kawada, J. Suzuki, M. Sase, A. Kaimai, K. Yashiro, Y. Nigara, J. Mizusaki, K. Kawamura, H. Yugami, *J. Electrochem. Soc.* 149 (2002) E252–E259.
- [29] C.R. Kreller, T.J. McDonald, S.B. Adler, E.J. Crumlin, E. Mutoro, S.J. Ahn, G.J. la O', Y. Shao-Horn, M.D. Biegalski, H.M. Christen, R.R. Chater, J.A. Kilner, *J. Electrochem. Soc.* 160 (2013) F931–F942.
- [30] J.-H. Lee, H. Kim, S.M. Kim, T.-W. Noh, H.-Y. Jung, H.-Y. Lim, H.-G. Jung, J.-W. Son, H.-R. Kim, B.-K. Kim, H.-J. Je, J.-C. Lee, H. Song, H.-W. Lee, *Adv. Energy Mater.* 2 (2012) 461–468.